LONG TERM EXPLORATION OF PLANETARY PITS, CAVES, AND LAVA TUBES

Virtual Conference 19–23 October 2020

Himangshu Kalita[1], Jekan Thangavelautham[2]

[1]Aerospace and Mechanical Engineering, University of Arizona, 1130 N Mountain Ave, Tucson, AZ, USA 85721, E-mail: hkalita@email.arizona.edu

[2]Aerospace and Mechanical Engineering, University of Arizona, 1130 N Mountain Ave, Tucson, AZ, USA 85721, E-mail: jekan@arizona.edu

ABSTRACT

Recently discovered pits on the surface of the Moon and Mars are theorized to be remnants of lava-tubes and their interior maybe in pristine condition. Current landers and rovers are unable to access these areas of high interest. However, multiple small, low-cost robots that can utilize unconventional mobility and can work as a team can be deployed to explore these environments. We proposed a spherical robot called SphereX that achieves mobility through hopping using a miniaturized propulsion system and a 3-axis reaction wheel system and power through either lithium-ion batteries or fuel cells. However, with this design architecture, SphereX has a limited lifetime. Hence, there is a need for systems that can survive for long durations inside these pits, caves, and lava tubes. In this paper, we provide alternative ways to enhance SphereX robots to survive inside these environments for long duration through mechanical hopping mechanisms for mobility and power beaming from a surface entity inside the caves and lava tubes with the help of lasers.

1 INTRODUCTION

There are evidence of subsurface voids and mare-pits on the lunar surface revealed from the high-resolution orbital imagery taken by the Lunar Reconnaissance Orbiter Camera (LROC) [1]. The dimensions of these pits vary widely and range in diameter from ~900 m to less than 5 m, with a median diameter of 16 m, and a median depth of 7 m. Mare pits tend to be larger than the impact melt pits, with the majority of mare pits being >40 m in diameter and >30 m deep [2]. Moreover, data from NASA's GRAIL mission has shown evidence of a vast network of empty lunar lava tubes that extends to tens of kilometers [3]. These environments are high priority targets and by exploring these environments, we can ascertain the range of conditions that can support life and identify planetary processes that are responsible for generating and sustaining habitable worlds [4].

We proposed in the past, a small, low-cost, modular spherical robot called SphereX that achieves unconventional mobility through hopping and rolling for exploring planetary pits, caves, and lava tubes [5] as shown in Fig. 1. SphereX has a mass of 1.5-4 kg and a diameter of 180-300 mm and contains space-grade electronics like computer board for command and data handling, power board for power management and radio transceiver for communication among multiple robots. Power is either stored through lithium-ion batteries or generated on demand using a fuel cell system and communication achieved through multiple UHF/S-band antennas. Mobility is achieved through a combined action of a miniaturized propulsion system and a 3-axis reaction wheel system in the form of combined ballistic hopping and rolling. Possible instruments may include a pair of FPGA cameras for imaging, a 3D LiDAR scanner for mapping, navigation and localization, and an impedance spectroscopy instrument to determine water content, distribution, and phase in regolith inside the caves, pits and lava tubes.

However, with this design architecture, SphereX has limited lifetime that ranges from days to weeks as battery charge for power and chemical propellants for mobility and fuel cell will run out. But there is a need for systems that can survive inside these pits, caves, and lava tubes for long duration. In this paper, we provide alternative ways to enhance SphereX robots to survive inside these environments for long duration. The need for chemical propellants for hopping can be eliminated by using mechanical hopping mechanisms for mobility which needs electrical power for operation. Moreover, the need to store power in lithium-ion batteries or the need for chemicals for fuel cell operation can be eliminated by beaming power from a surface entity inside the caves and lava tubes with the help of lasers. These technologies and modifications to SphereX will make them a viable candidate for long term exploration of planetary pits, caves and lava tubes.

2 LINE OF SIGHT ANALYSIS

To feasibly explore a cave or lava tube requires a team of SphereX robots that work collaboratively to map, navigate and communicate the data back to the base

station. Often, there will not be line of sight communication between the base station and the robot team. Hence, the robots need to act as relays to pass messages from the base station to individual robots along the cave much like a bucket-brigade. Moreover, these team of robots will also be used to transmit power wirelessly by beaming a high-power laser from a surface entity to the robots inside the cave. Each robot will be equipped with photo voltaic (P-V) panels for receiving the incident laser. The P-V panels can also be used as a receiver for optical communication [6].

For the architecture of deploying multiple SphereX robots assisted by a large rover or a lander to work, a direct line-of-sight connection link from the base system on the surface of the pit to the farthest robot inside the pit should be maintained. This section provides an analysis on the feasibility of maintaining such a connection link from a base system on the surface of the pit with another SphereX robot on the floor of the pit.

2.1 Line-of-sight from pit surface to pit floor

With the line-of-sight architecture defined above, the base system on the surface of the pit needs to maintain a direct line-of-sight connection link with the SphereX robot on the floor of the pit entrance. To maintain a direct line-of-sight connection link the system on the surface near the pit entrance at a distance a deploys a boom of height h vertically upwards that consists of a transmitter at its tip. The transmitter has a beam width B and is oriented at an angle ϕ with respect to the boom as shown in Fig. 1. The distance d on the floor of the pit within which a direct line-of-sight communication link is possible with the base system on the surface is calculated by projecting the beam width of the transmitter on the floor. The dimensions of the pit entrance are also shown in Figure 1.

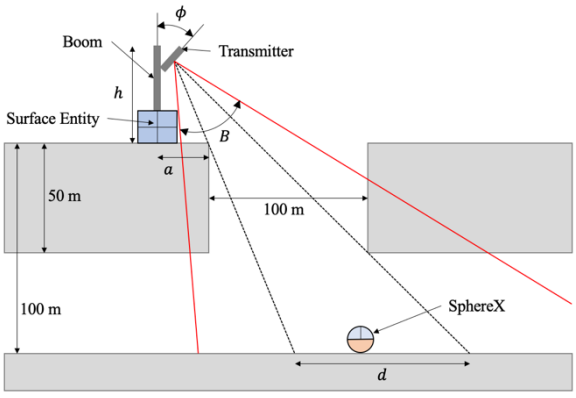

Figure 1: Description of the boom deployed by the base system on the surface near a pit entrance with a transmitter at its tip. The dimensions are not scaled.

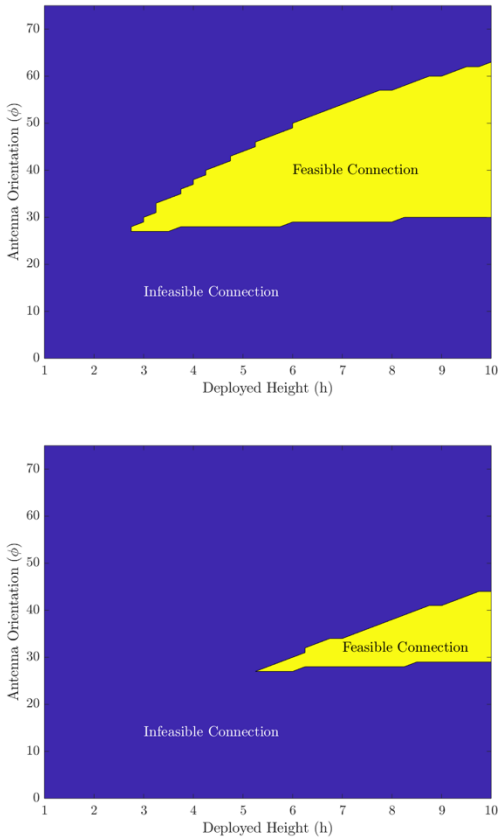

Figure 2: Variation of feasible direct line-of-sight communication link for an optical transmitter with respect to the deployed boom height h and orientation of the transmitter ϕ for (Top) $a = 5m$, (Bottom) $a = 10m$.

Figure 2 shows the feasibility of a direct line-of-sight communication link with respect to the deployed boom height h in meters and orientation of the transmitter ϕ in degrees for an optical transmitter where the angle $B \rightarrow 0$. The parameters used for the results are Fig. 2 (Top): $a = 5$m, and Fig. 2 (Bottom): $a = 10$m. It can be seen that when the surface entity is deployed within 5m of the entrance, a boom of 3m will be sufficient to maintain a direct line-of-light communication link with another SphereX on the floor of the pit, while when its deployed at a distance of 10m the minimum required boom height increases to 5.7m.

3 POWER OPTIONS

With the absence of solar power inside planetary pits, caves and lava tubes, two power sources that had been analyzed before for the design of SphereX are lithium-ion batteries and PEM fuel cells [8]. Lithium-ion batteries store power required for the entire mission while fuel cells generated power on demand. To avoid

cryogenic storage of hydrogen and oxygen for the operation of the fuel cells, hydrogen is produced on demand through the hydrolysis of LiH and oxygen is produced through the catalytic thermal decomposition of $LiClO_4$. Figure 3 shows a comparison between lithium-ion batteries and PEM fuel cells in terms of mass.

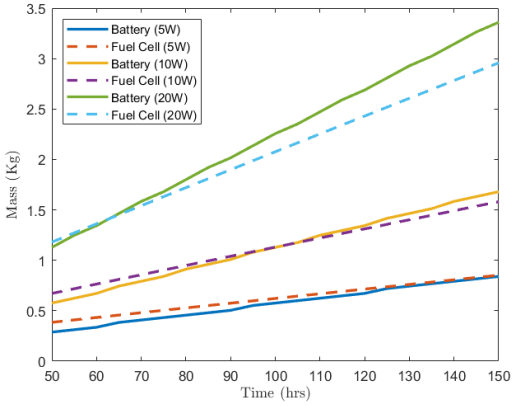

Figure 3: Comparison of lithium-ion battery and fuel cell in term of mass over mission duration for varying power demand.

Although PEM fuel cells outperform lithium-ion batteries as the mission duration and power demand increases, but still its operation is limited by the amount of LiH and $LiClO_4$ carried for its operation. As such we need alternate power options for a long duration exploration mission. With multiple robots laid down along a cave/lava tube, we propose to transfer power wirelessly by beaming a high-power laser from a base station on the surface to the robots inside the cave through a multi-hop channel. Each robot will be equipped with photo voltaic (P-V) panels for receiving and a gimballed reflector for reflecting the incident laser. The P-V panels can also be used as a receiver for optical communication as shown in Figure 4. A self-reverse bias is applied to the solar panel to improve its performance by increasing the number of photocarriers and improving drift velocity. The energy harvesting branch is connected to the EPS system that supplies the rated current and voltage to the battery for charging. The boost converter is connected to the EPS system to supply a high reverse bias to the solar panels. The signal from the communication branch is provided to the analog to digital converter which is processed by the microcontroller for telemetry data.

Wireless power transfer through laser is modeled in three phases a) Electricity to laser conversion where electrical power input is converted into laser, b) Laser transmission where laser power is attenuated while traveling through a medium, and c) Laser to electricity conversion where laser is converted into electrical power by photo voltaic panels.

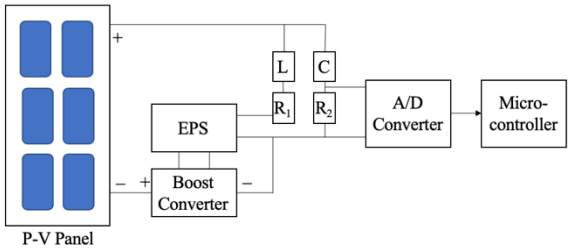

Figure 4: Photo voltaic panel self-reverse biased receiver circuit for laser communication and power transfer.

3.1 Electricity to laser conversion

Electrical power P_s is provided by a power supplier to the laser transmitter, which depends on the current I_t and voltage V_t such that $P_s = I_t V_t$. The supply power stimulates the gain medium to generate laser of power P_l which relies on current I_t as shown in Equation (1).

$$P_l = \zeta \frac{h\nu}{q}(I_t - I_{th}) \tag{1}$$

Where, ζ is the modified coefficient, h is the Plank's constant, ν is the laser frequency, q is the elementary charge constant, and I_{th} is the current threshold. Thus, the electricity to laser conversion efficiency is given as Equation (2).

$$\eta_{E-L} = \frac{P_l}{P_s} \tag{2}$$

3.2 Laser transmission

Laser power is attenuated when transmitted over large distances while propagating through a medium and the attenuation coefficient α is modeled as Equation (3).

$$\alpha = \frac{\sigma}{\kappa}\left(\frac{\lambda}{\chi}\right)^{-\rho} \tag{3}$$

Where, λ is the wavelength of the laser, σ and χ are two constants, κ is the visibility, ρ is the size distribution of the scattering particles which depend on the visibility. The laser transmission efficiency is then defined as Equation (4).

$$\eta_T = e^{-\alpha d} \tag{4}$$

Where, d is the distance.

3.3 Laser to electricity conversion

Under laser illumination of incident power P_i, the short circuit current I_{sc} of a photovoltaic cell is given by Equation (5).

$$I_{sc} = \frac{qP_i}{h\nu} QE \quad (5)$$

Where, QE is the external quantum efficiency at the wavelength of interest and for higher efficiency solar cells, the quantum efficiency is very close to unity. The I-V curve model of solar cells is given by Equation (6).

$$I = I_{sc} - I_{sat}\left[exp\left(\frac{V + R_s I}{V_T}\right) - 1\right] - \frac{V + R_s I}{R_{sh}} \quad (6)$$

Where, I is the operating current, V is the operating voltage, $V_T = nkT/q$, n is the diode factor, k is the Boltzmann constant, T is the temperature, R_s is the series resistance, and R_{sh} is the shunt resistance of the solar cell (R_s is assumed to be small and neglected). Thus, the laser to electricity conversion efficiency is defined as Equation (7).

$$\eta_{L-E} = \frac{IV}{P_i} \quad (7)$$

Based on the above analysis, the laser power transmission efficiency from the power supplier at the transmitter to the power output at the receiver is defined as Equation (8).

$$\eta_{PT} = \eta_{E-L}\eta_T\eta_{L-E} \quad (8)$$

3.4 Power transfer over a multi-hop channel

For power transfer inside a cave with the shape of the cave and obstacles making it impossible to maintain a direct-line-of-sight connection over distance, a multi-hop channel is proposed where the laser beam is relayed from one point to another point through multiple sensors in between. The sensors are modeled as reflectors

Reflectors: The reflectors receive the incident laser power from its previous neighbor and instead of converting all the laser power into electrical power, it converts only a fraction of it for storage and reflects the rest to the next neighboring sensor. The laser power transmitted by the source, $P_{l(0)}$ for supplied power, P_s is expressed as:

$$P_{l(0)} = \eta_{E-L} P_s \quad (9)$$

The incident laser power received by the photovoltaic panels of the n^{th} sensor is expressed as:

$$P_{i(n)} = \eta_T P_{l(n-1)} \quad (10)$$

The electrical power produced by the n^{th} sensor is then expressed as:

$$P_{e(n)} = \eta_{L-E} P_{i(n)} \quad (11)$$

If the efficiency of reflection is defined as η_R, and each sensor stores P_{sensor} power, the laser power transmitted by the n^{th} sensor to the $(n+1)^{th}$ sensor is expressed as:

$$P_{l(n)} = \eta_R \left(P_{e(n)} - \frac{P_{sensor}}{\eta_{L-E}}\right) \quad (12)$$

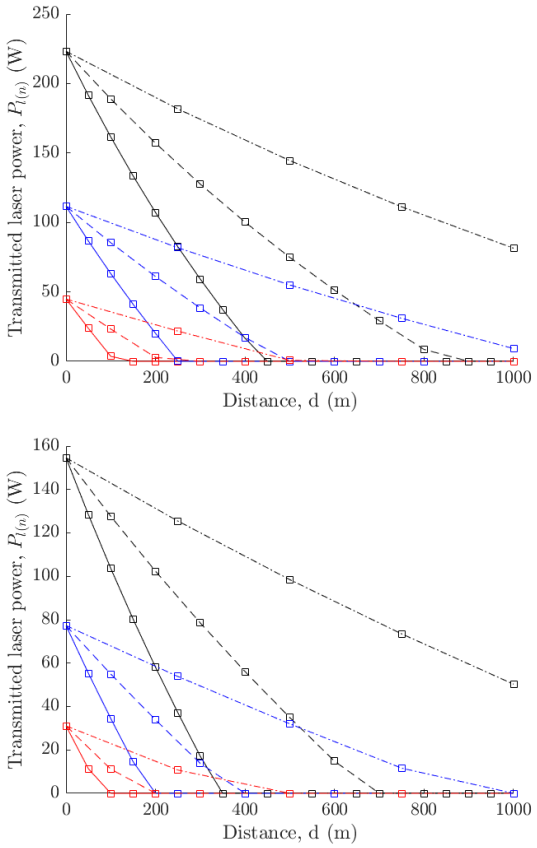

Figure 5: Variation of transmitted power by each robot placed at a distance $d = [50, 100, 250]m$, over a total distance of 1000m for an initial supply power of $P_s = [100, 250, 500]W$. The wavelength of the laser is (Top) 810nm, (Bottom) 1550nm.

Figure 5 shows the variation of transmitted power by each robot placed at a distance of $d = [50, 100, 250]$ m, over a total distance of 1000 m for lasers with wavelength 810 nm and 1550 nm respectively. For each distance d and wavelength, the model was simulated for 3 values of initial power supply $P_s = [100, 250, 500]$ W and each sensor stores a power of $P_{sensor} = 10$ W. Table 1 shows the description of the legend for Figure 5.

Table 1: Legend for Figure 5.

LineSpec	Property
Color – 'red'	$P_s = 100W$
Color – 'blue'	$P_s = 250W$
Color – 'black'	$P_s = 500W$
LineStyle – 'Solid'	$d = 50m$
LineStyle – 'Dashed'	$d = 100m$
LineStyle – 'Dash-dot'	$d = 250m$

4 MOBILITY OPTIONS

SphereX achieves mobility through ballistic hopping and controlled rolling with the help of a miniaturized propulsion system and a 3-axis reaction wheel system. Hopping with the help of a propulsion system is energy efficient, provides range and also provides SphereX the ability to perform soft landing hopping maneuvers. This soft-landing hopping maneuver is important when the robot hops over a large distance and specially to land on a pit floor from the surface which is approximately 100m deep. However, SphereX has limited capacity to store propellants and hence not viable for long-term exploration missions. As such there is a need for alternative mobility mechanism that operates on electrical power. Two mobility options we consider here are: a) Hopping with a spring based mechanical system and b) Hopping with reaction wheels.

4.1 Spring-based mechanical hopping mechanism

Although there are a wide variety of mechanical hopping mechanisms designed for planetary exploration robots, here we analyze the most commonly used mechanism: spring and gear based hopping mechanism. In this mechanism, a gear actuated by an electric motor is used to compress and store energy on a spring, and then the stored energy is converted to kinetic energy of the robot with the help of a foot for hopping mobility [9]. A simplified model is developed for the hopping process as shown in Figure 6. The first step is to compress the spring to store energy $E_0 = k\Delta x^2/2$ (where, k is the spring constant and Δx is the displacement of the spring), the next step is to orient the robot at a desired angle and the last step is to release the stored energy causing the robot to hop. A 3-axis reaction wheel system is used to orient the robot to its desired orientation. During the last step, the body of the robot first accelerates upward due to the spring force, while the lower part remains stationary. Once the body moves to a specific height, a perfect inelastic collision happens between the body and the foot if the spring constant is large. After the collision, both parts move with the same velocity, which is the robot's take-off velocity v_0. Let the mass of the body be m_b and that of the foot be m_f. In the ideal case, all the energy E_0 stored in the spring is converted to the kinetic energy of the body. Therefore, the speed of the body before the inelastic collision is $v_b = \sqrt{2E_0/m_b}$. By the conservation of momentum, $m_b v_b = (m_b + m_f)v_0$, thus

$$v_0 = \frac{\sqrt{2m_b E_0}}{m_b + m_f} \tag{13}$$

With the take-off angle equal to θ and acceleration due to gravity g, the distance hopped d_{hop} can be obtained as Equation (14).

$$d_{hop} = \frac{2E_0 \sin 2\theta}{(1+r)mg} \tag{14}$$

where, $r = m_f/m_b$ and $m = m_f + m_b$.

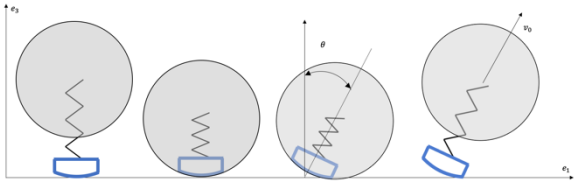

Figure 6: Simplified model of exchange of energy for the hopping process.

The electrical power consumed by the motor for each hop is then calculated as:

$$P_m = \left(i_0 + \frac{\mathfrak{m}}{k_T}\right)V \tag{15}$$

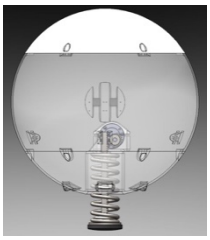

Figure 7: CAD model of the mechanism

where, i_0 is the no load current, k_T is the torque constant, V is the operating voltage of the robot, and $\mathfrak{m}$ is the maximum torque required by the pinion gear to compress the spring. Moreover, electrical power is consumed by the reaction wheel system to orient the robot which is calculated as $P_{rw} = \tau_{rw}\omega_{rw}$, where τ_{rw} is the torque applied and ω_{rw} is the angular velocity of the reaction wheel system. As such, the total power consumed is $P_S = P_m + P_{rw}$. Figure 8 shows the energy required and peak power required during the operation of the motor as a function of hopping distance on the surface of the Moon.

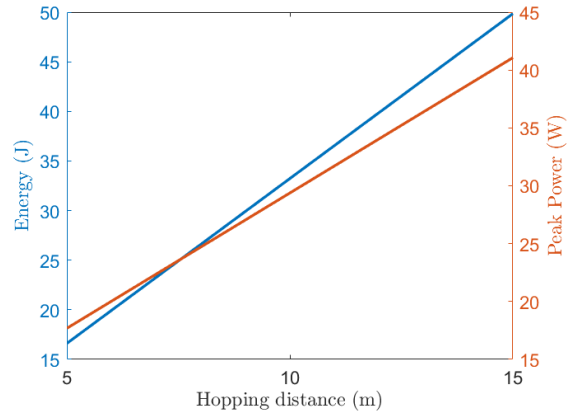

Figure 8: Energy and peak power required for hopping using the spring-based mechanism on the surface of the Moon.

4.2 Reaction wheel-based hopping mechanism

Hopping can also be achieved with three reaction wheels by slowly accelerating (spin-up phase) and then impulsively braking (braking phase) them to produce reaction force on the external spikes [10]. The maximum distance the robot can hop with this system is calculated as Equation (16).

$$d_{hop} = \frac{h_{rw}^2 \eta^2 l^2 \sin(2\alpha)}{g} \tag{16}$$

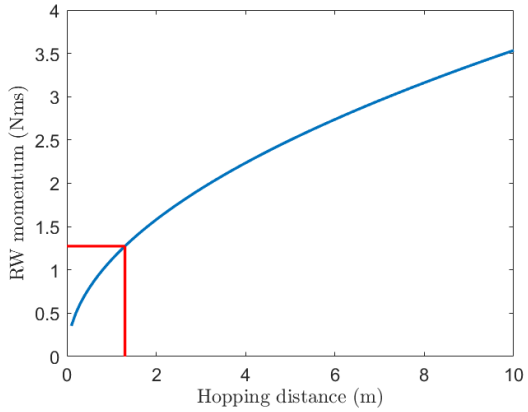

Figure 9: Reaction wheel angular momentum required for hopping using the reaction wheel-based mechanism on the surface of the Moon.

Where, h_{rw} is the reaction wheel angular momentum, l is the length of each spike from the robot's center of mass, 2α is the angle between two successive spikes and $\eta = 1/(J_s + ml^2)$, where J_s is the robot's inertia and m is the robot's mass. Figure 9 shows the reaction wheel angular momentum required as a function of hopping distance on the surface of the Moon. The red lines show the limit on reaction wheel angular momentum and hopping distance based on the maximum angular momentum provided by COTS reaction wheel system that can fit inside a SphereX robot. As such this mechanism is suited for longer hopping distance compared to the spring-based mechanism.

With a mechanical hopping mechanism, although the robots will be able to achieve mobility for longer durations, but they will lose their ability to perform soft-landing maneuvers while entering the pit from the surface. As such alternative mechanisms are required for the robots to survive while entering the pits. One idea is to attach pallets of solid rockets to each robot that would allow one soft landing maneuver which will be analyzed later.

5 THERMAL CONTROL

In order to prevent the robot from freezing and overheating without compromising thermal reliability and stability, we implement a thermal model that relies on both active and passive thermal control elements as shown in Figure 10. The proposed thermal model relies on a low emissive silver coating finish and a low conductive silica aerogel insulation layer along with thermal control heat rejection/generation mechanism composed of a variable emittance coating (VEC), a heat switch and an electric heater. The model consists of a spherical shell of mass m_s and specific heat $c_{p,s}$, representing the robot shape, with a low outer emissivity coating (ϵ_s) and a thick inner insulation layer with conductivity (λ_{in}). The temperature of the outer shell is represented as T_s, and that of the surrounding as T_a. All the internal components of the robot are assumed to be a homogeneous spherical body with temperature T_b, mass m_b and specific heat $c_{p,b}$. The VEC has a maximum emissivity of $\epsilon_{s,vec}$ and a surface area of A_{vec}. The heat switch has a thermal conductivity λ_{sw}, contact area A_{sw}, and switch length x_{sw}. Moreover, heat is generated during the operation of the robot by different subsystems (mobility, power, communication, electronics) which is denoted by $\dot{Q}_{gen}$. As such we implement the thermal model with two state variables T_b and T_s and the differential equations governing them is shown in Equation (17).

$$m_b c_{p,b} \dot{T}_b = \dot{Q}_{gen} - \dot{Q}_{cond,s} - \dot{Q}_{cond,g} - \dot{Q}_{cond,sw} + \dot{Q}_{eh}$$

$$m_s c_{p,s} \dot{T}_s = \dot{Q}_{sun} + \dot{Q}_{cond,s} - \dot{Q}_{rad,[vec]} - \dot{Q}_{conv} \tag{17}$$

Figure 11 shows the body temperature of the robot inside a lunar lava tube with surrounding temperature $T_a = 248K$. It can be seen that the robot was able to maintain its desired temperature of 300K using the thermal control model described.

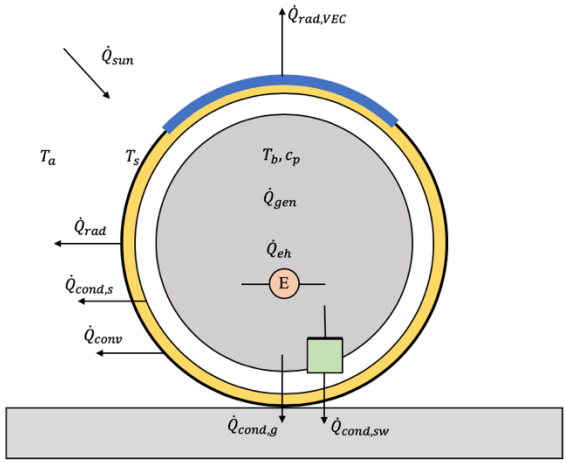

Figure 10: Modes of heat transfer involved.

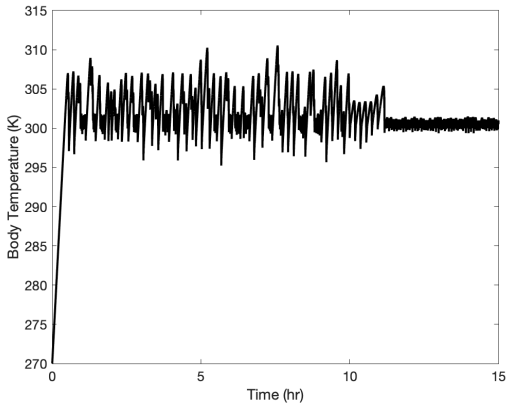

Figure 11: Body temperature of SphereX over time inside a lunar lava tube.

6 CONCLUSIONS

In this paper we outlined strategies for long term exploration of planetary pits, caves, and lava tubes using multiple small, low-cost spherical robots SphereX. For long term exploration of these environments using SphereX, power and mobility are the two main limiting factors. The baseline design of SphereX uses propulsion based hopping mechanism for mobility and lithium-ion battery/fuel cell-based power system which has limited capacity in terms of mission lifetime. As such we proposed using lasers to transmit power from the surface to the robots inside a cave or a lava tube through a multi-hop channel. Each robot will be equipped with receivers and reflectors which they use to charge their respective batteries and then reflect the rest to the nearest robot. Moreover, to avoid using a propulsion based hopping mechanism, we proposed using mechanical hopping mechanism that needs only electrical power for its operation. In addition to that we presented a brief thermal model of the robot for it to survive inside these environments. Our initial simulations show feasibility of our proposed idea for long-term exploration of these environments but needs further detailed analysis.

References

[1] M. Robinson, et al., (2012) "Confirmation of sublunarean voids and this layering in mare deposits," Planetary and Space Science 69, pp. 18-27.

[2] R. V. Wagner and M. S. Robinson, "Distribution, formation mechanisms, and significance of lunar pits," Icarus, Vol. 237, pp. 52-60, 2014.

[3] Chappaz, L., Sood, R., Melosh, H. J., et al. (2016). "Evidence of large empty lava tubes on the Moon using GRAIL gravity." Geophysical Research Letters, 44(1).

[4] National Research Council 2011. Vision and Voyages for Planetary Science in the Decade 2013-2022. Washington, DC: The National Academies Press.

[5] J. Thangavelautham, M. S. Robinson, A. Taits, T. J. McKinney, S. Amidan, A.Polak, "Flying, hopping Pit-Bots for cave and lava tube exploration on the Moon and Mars," 2nd International Workshop on Instrumentation for Planetary Missions, NASA Goddard, Greenbelt, Maryland, 2014.

[6] H. Kalita, L. Vance, J. Thangavelautham, "Laser Beam for External Position Control and Traffic Management of On-Orbit Satellites," Provisional Patent, US 62/731,399, 2018.

[7] Kalita, H., and Thangavelautham, J., "Multidisciplinary Design and Control Optimization of a Spherical Robot for Planetary Exploration," AIAA SciTech Forum, Orlando, 2020.

[8] Kalita, H., Jameson, T. M., Stancu, G., and Thangavelautham, J., "Design and Analysis of a Mechanical Hopping Mechanism Suited for Exploring Low-gravity Environments," IEEE Aerospace Conference, Big Sky, 2020, pp. 1-10.

[9] R. Allen, et al., "Internally-actuated rovers for all-access surface mobility: Theory and experimentation," IEEE International Conference on Robotics and Automation (ICRA), 2013.